Performance Analysis Under Double Sided Clipping and Real Time Implementation of DCO-GFDM in VLC Systems

Vejandla Kishore ⓘ, *Student Member, IEEE*, Siva Prasad Valluri, *Student Member, IEEE*,
Venkata Mani Vakamulla ⓘ, *Senior Member, IEEE*, Mathini Sellathurai ⓘ, *Senior Member, IEEE*,
Abhinav Kumar, *Senior Member, IEEE*, and Tharmalingam Ratnarajah ⓘ, *Senior Member, IEEE*

Abstract—In the context of visible light communications (VLC), DC biased optical generalized frequency division multiplexing (DCO-GFDM) is a recently emerged waveform relying on block based transmission and employs pulse shaping using a circularly rotating prototype filter. In this work, we analyze the bit error rate (BER) performance of DCO-GFDM under double sided clipping induced by front end light emitting diode (LED) transmitters. The effect of clipping on BER performance is studied under different biasing conditions for different prototype filters. Additionally, we experimentally verify the real time performance of DCO-GFDM using different pulses. Simulations are performed in MATLAB software and experiments are conducted in a Lab-view environment using hardware. Two independent universal software radio peripherals (USRP)s are utilized as transmitter and receiver boards. It is observed that the simulation results match well with the corresponding theoretical results. Meanwhile, the experimentally achieved results for error vector magnitude (EVM), the received constellations, and the received spectrum along with BER in different cases are presented for the validation of DCO-GFDM waveform and are compared with DCO orthogonal frequency division multiplexing (DCO-OFDM).

Index Terms—Bit error rate (BER), DC biased optical generalised frequency division multiplexing (DCO-GFDM), error vecor magnitudes (EVM), universal software radio peripherals (USRP), visible light communications (VLC).

I. INTRODUCTION

THE upsurge in the need for surplus data rates has proliferated the necessity for an alternative to the overcrowded Radio Frequency (RF) spectrum in the field of wireless communications. Therefore, Visible Light Communications (VLC) that utilize gigantic visible spectrum has been explored by the researchers to buttress the existing RF spectrum. Unlike RF, VLC has created its impact with its distinctive benefits like huge unlicensed bandwidth, secure data transmission, insusceptible to electromagnetic interference, and energy efficiency that is achieved due to the exploitation of existing Light Emitting Diodes (LED) infrastructure. The inherent high speed switching property of LEDs has made them suitable for communication along with illumination in indoor environments using VLC technology [1], [2].

To transmit information, a VLC system relies on Intensity Modulation (IM) and Direct Detection (DD) principle which restricts the transmitted signal to become unipolar. Though the single carrier modulations can easily be implemented, higher data rate and many other requirements open the path of the investigation into several variants of multi carrier modulation waveforms based on Orthogonal Frequency Division Multiplexing (OFDM) that fulfil the necessities of VLC systems [3]. Notably, all these Optical OFDM (O-OFDM) variants are lagging in terms of either spectral efficiency or power efficiency, and employ rectangular pulse shaping in time domain due to which the Out-of-Band (OOB) emission in the frequency domain is increased. Further, the high value of Peak-to-Average Power Ratio (PAPR) in the O-OFDM schemes, causes the signal to be distorted more at the front end non-linear devices. In addition to these, the upcoming high speed 5 G systems need flexibility in the waveform generation to meet the requirements of VLC based vehicular communication technology [4], [5]. All these challenges arise the necessity for an alternative multicarrier waveform that retains the benefits of O-OFDM variants and address the aforementioned issues.

So, to fulfill these requirements amicably, a new waveform named DC biased Optical Generalized Frequency Division Multiplexing (DCO-GFDM) waveform has been initiated in [6], [7], by transmitting multiple symbols on each sub-carrier. Unlike in O-OFDM variants, DCO-GFDM transmits symbols by dividing
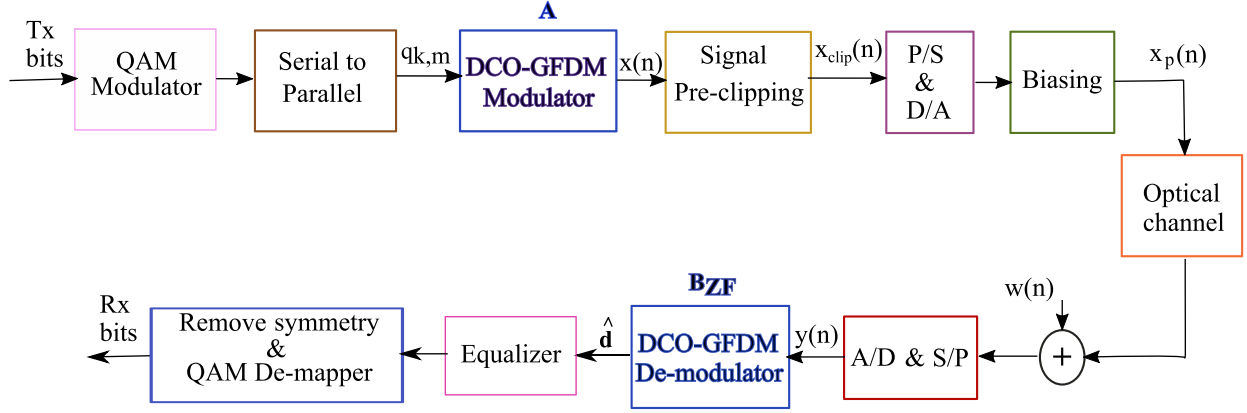
Fig. 1.   Block diagram of the DCO-GFDM based IM/DD system.

both time and frequency grids and meticulously pulse shaping with a circular rotating filter. By doing so, DCO-GFDM enable each sub-carrier to transmit multiple symbols which is different from OFDM modulation where each subcarrier transmit one symbol. Specifically, in the modulation process Square Root Raised Cosine (SRRC) pulse with roll-off factor (α) is used as a circularly rotating pulse shaping filter whose side lobes can be controlled by changing α. These side lobes contribute significantly to the amount of energy dissipated into the adjacent bands. By varying the roll-off factor, the depth of the side lobes and the width of the main lobe can be varied which in turn give control over the OOB emission and PAPR. Thus, the benefits like spectral efficiency improvement, reduction in PAPR, and OOB emission are attained by using DCO-GFDM when compared with the popular O-OFDM waveforms. Furthermore, DCO-GFDM system provides the advantage of flexibility in the modulation, which is not present in OFDM based waveforms.

Nevertheless, the non-linear behavior of the front end LED transmitter devices affect the performance of any waveform in a VLC system. The unipolar constraint on the signal and the power rating of the LED together make the time domain signal to be clipped at both ends [8]. In [8], the effect of the clipping model is studied on the performance of optical OFDM based systems where only the frequency plane is divided and the time plane is undivided in the time frequency plane. In contrast to OFDM systems, this work considered the effect of double sided clipping noise model on the GFDM based system where both time and frequency planes are divided along with circular pulse shaping with a flexible prototyping filter which effect the signal power as given in the subsequent sections. This double sided clipping of the signal will affect the systems Bit Error Rate (BER) performance and is investigated in the present study for the DCO-GFDM based system with various pulse shaping filters under different constraints. Although the analytical study gives a preliminary understanding of the system, it is essential to examine a real time system to interpret the performance. In recent times, Universal Software defined Radio Peripheral (USRP) based testbeds are gaining popularity due to their effectiveness in the execution of real time systems. In our earlier works, a GFDM based RF test bed and a VLC test bed to validate two novel O-OFDM waveforms have been designed [9], [10]. For

the first time in the literature, we are presenting a VLC testbed designed using DCO GFDM system under different constraints. Moreover, we demonstrate the performance of DCO-GFDM in terms of the received constellations, Error Vector Magnitude (EVM), BER, and the received spectrum in comparison with the popular DCO-OFDM system.

The rest of the paper is sectioned as follows. Section-II describes the proposed system transmitter and receiver. Section-III performs the comparative analysis for the proposed modulation with existing techniques. Section-IV presents the simulation results and Section-V concludes the paper.

II. GFDM BASED VLC SYSTEM MODEL

In this section, we present the complete system model of DCO-GFDM signal following the requirements of VLC systems and draw all the useful parameters relating to the power constraints of non-linear LED transmitters that come as front end devices in VLC systems. The DCO-GFDM system model considered in the present work is shown in Fig. 1. Initially, the intended transmitter bits are mapped by the QAM mapper and will be given to the DCO-GFDM modulator whose details are shown in Fig. 2. DCO-GFDM is a multicarrier modulation waveform relying on block based transmission that retains all the benefits from OFDM variants and provides flexibility in its generation. If we look at the case of DC biased Optical OFDM (DCO-OFDM) where each sub-carrier transmits only one symbol, there are $\frac{K}{2} - 1$ effective symbols on K number of sub-carriers excluding the Hermitian symmetrical symbols. Coming to the block based transmission in DCO-GFDM, a block of symbols $N = MK$ is divided into K sub-carriers with each sub-carrier transmitting M sub-symbols. In order to attain the time domain DCO-GFDM signal $x(n)$ with a predefined variance $\sigma_{x(n)}^2$ the enabled sub-carriers $q_{k,m}$ should be scaled by a, which is given according to the Parseval theorem as,

$$a = \sigma_{x(n)} \sqrt{\frac{M(K-1)}{\sum_{m=0}^{M-1} \sum_{k=0}^{K-1} |q(k,m).p_{mK}|^2}}, \qquad (1)$$

where, p_{mK} is a filter $p(n - mK), n \in 0, 1, \ldots, MK - 1$ that is circularly rotated by K for every m. The scaling factor a is used to obtain the scaled symbols $d_{k,m}$ from which we get the
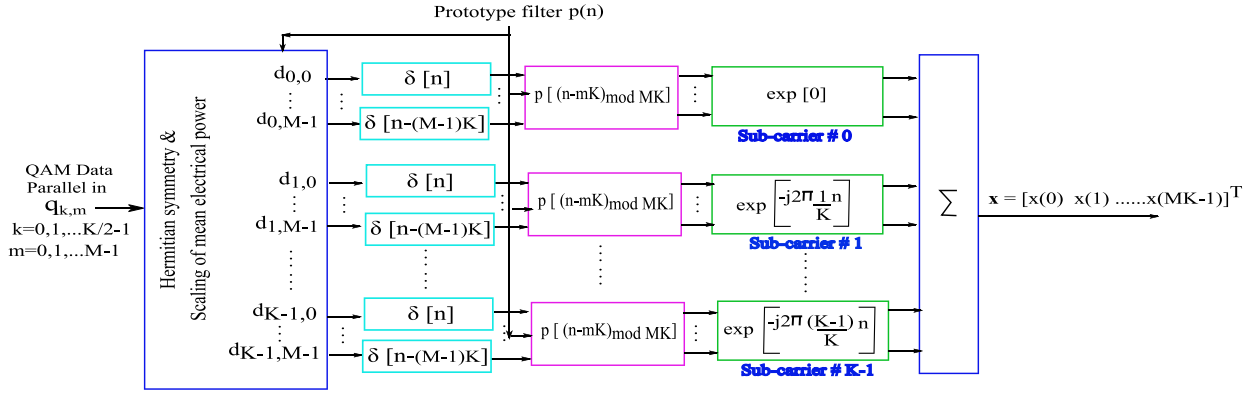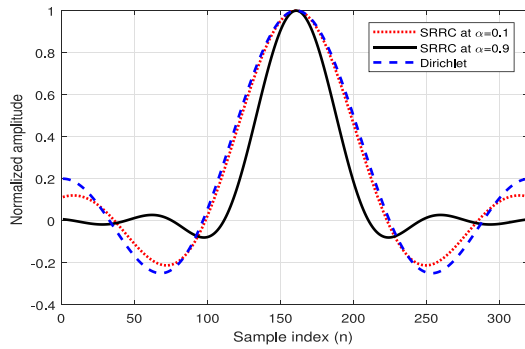
Fig. 2.   Details of DCO-GFDM modulator.

Fig. 3.   Time domain plots of employed prototype pulses.

real DCO-GFDM signal as [6], [11],

$$x(n) = \sum_{k=0}^{K-1} \left(p(n) \exp(j2\pi \frac{k}{K} n) \right) \circledast d_k[n], \qquad (2)$$

where, $\circledast$ represents circular convolution and $p(n)$ is the long length prototyping filter. In the current work, SRRC pulse with roll-off factor α and Dirchlet pulses are employed. The Dirichlet pulses are generated by employing an MK point inverse Fourier transform on the rectangular pulse $r(i)$, for $i \in 0, 1, \ldots, MK-1$, having unity samples from $i \in 0, 1, \ldots, M-1$ and zero for the remaining. Unlike SRRC pulse that spoils orthogonality among the sub-carriers in DCO-GFDM, Dirichlet pulse improves the performance by retaining the orthogonality among the sub-carriers. The plot of the Dirichlet pulse along with SRRC are shown in Fig. 3. Further, $d_k[n], n \in 0, 1, 2, \ldots, N-1$ is obtained by oversampling the scaled Jth ary-QAM (J-QAM) symbols $d_{k,m}$ for every m like as shown in Fig. 2, which is given by,

$$d_k[n] = \sum_{m=0}^{M-1} d_{k,m} \delta[n - mK]. \qquad (3)$$

To get the real signal as per the VLC system constraint, Hermitian symmetry is applied on the unscaled QAM symbols $q_{k,m}$. The Hermitian symmetry arrangement that is also retained in the scaled QAM symbols which are $K \times M$ blocked in $d_{k,m}$ can

be represented as follows.

$$\{d_{k,m}\}_{k=0}^{K-1} = \left[d_{0,m} \quad \{d_{k,m}\}_{k=1}^{\frac{K}{2}-1} \quad d_{\frac{K}{2},m} \quad \{d_{k,m}^*\}_{k=\frac{K}{2}-1}^{1} \right], \qquad (4)$$

in which $d_{0,m}$ and $d_{\frac{K}{2},m}$ are set to zero for all m to satisfy Hermitian symmetry. By collecting all the samples in (2) from $n \in 0, 1, \ldots, N-1$ into a vector $\mathbf{x} = [x(0), x(1), \ldots, x(N-1)]^\top$ of size $N \times 1$, the real DCO-GFDM signal can be conveniently represented in matrix form as [6], [11],

$$\mathbf{x} = \mathbf{A}\mathbf{d}. \qquad (5)$$

In (5), the modulation matrix $\mathbf{A}$ is given by,

$$\mathbf{A} = [p_{0,0}(n) \cdots p_{K-1,0}(n) \ p_{0,1}(n) \cdots p_{K-1,M-1}(n)], \qquad (6)$$

where

$$p_{k,m}(n) = p_{mK}.\exp\left(j2\pi \frac{k}{K} n\right) = p[(n - mK)_{\text{mod } MK}]$$
$$.\exp\left(j2\pi \frac{k}{K} n\right),$$

is a column sequence containing $N = MK$ samples from $n \in 0, 1, \ldots, N-1$. That means, in the modulation matrix $\mathbf{A}$, each column has N samples and there are N such columns which is obvious from $p_{k,m}(n)$ where the indices k and m are varying as $k \in 0, 1, \ldots, K-1$ and $m \in 0, 1, \ldots, M-1$ simultaneously. Therefore, with $N = MK$ number of columns with N samples in each column, the modulation matrix $\mathbf{A}$ becomes $N \times N$ and posses all the operations related to circular pulse rotation and transform operation as given in (2) and (3). In (5), $\mathbf{d}$ is the $N \times 1$ data vector given by $\mathbf{d} = [\mathbf{d}_0 \ \mathbf{d}_1 \ldots \mathbf{d}_{M-1}]^\top$ in which each $\mathbf{d}_m = \{d_{k,m}\}_{k=0}^{K-1}$ is a $1 \times K$ vector as given in (4). Thus, the real GFDM signal is generated using (5) to which proper biasing is applied before transmission according to LED constraints that are identified below.

Generally, at this stage, a Cyclic Prefix (CP) is added to overcome the channel impairments. However, the impact of CP in optical wireless systems is shown negligible on the electrical Signal-to-Noise Ratio (SNR) [8]. Therefore, CP is omitted in the following analytical presentation. Now coming to the front end non-linear LEDs through which we transmit the modulated

signal possesses a limited linear dynamic range and needs to be effectively utilized. To make use of the narrow dynamic range, the modulated signal should undergo pre-clipping before transmission. At that point, the pre-clipping is assumed in terms of power since the LED radiates optical power following forwarding current [8], [12]. With this in mind, the LED is considered to have a linear dynamic range between a minimum optical power P_{min} and a maximum optical power P_{max} points. Additionally, the biasing optical power P_{bias} is considered as essential for biasing the modulated signal. Further, the average optical power after pre-clipping the signal should not exceed the mean average optical power P_{mean} as per eye safety norms. In DCO-GFDM, the frequency domain symbol structure is similar to DCO-OFDM, and hence, the front end biasing parameters $\sigma_{x(n)}$ and P_{bias} in accordance with the dynamic range (P_{min}, P_{max}) are assumed similar to DCO-OFDM in [8], [12]. Hence, the clipping levels are set at $e_{bottom} = P_{min} - P_{bias}$ for bottom clipping level and $e_{top} = P_{max} - P_{bias}$ for top clipping level, which may become either positive or negative with the inequality $e_{bottom} < e_{top}$ being satisfied. The ideal case with least signal clipping would be $e_{bottom} = -\infty$ and $e_{top} = +\infty$. The pre-clipping showed in Fig. 1 can be applied according to [8], [12],

$$x_{clip}(n) = \begin{cases} e_{top}, & \text{if } x(n) \geq e_{top} \\ x(n), & \text{if } e_{bottom} < x(n) \leq e_{top} \\ e_{bottom} & \text{if } x(n) \leq e_{bottom}. \end{cases} \quad (7)$$

Post the pre-clipping, a bias P_{bias} is applied to the signal and transmitted through the LED transmitter. At the receiver by using Bussgang Theorem and Central Limit Theorem (CLT) [13], [14], the received signal vector $\mathbf{y} = [y(0)\ y(1) \ldots y(N-1)]^\top$ with clipping noise vector ($\mathbf{w_{clip}}$) and Additive White Gaussian Noise (AWGN) noise vector ($\mathbf{w}$) can be modelled as,

$$\mathbf{y} = g_{opt}K_f\mathbf{x} + g_{opt}\mathbf{w_{clip}} + \mathbf{w}. \quad (8)$$

It should be noted that (8) is written in terms of unclipped signal $\mathbf{x}$ attenuated by a factor K_f due to clipping. The clipped noise component is separated into an uncorrelated non-Gaussian component $\mathbf{w_{clip}}$ which has a variance of σ_{clip}^2. Further, the AWGN noise vector $\mathbf{w}$ is assumed to have a variance of σ_w^2. In (8), g_{opt} is the optical path gain coefficient defined in terms of average irradiance of photodiode as in [6]. The attenuation factor K_f can be derived using a similar approach used for DCO-OFDM in [8], [12]. At this stage, to get the estimated scaled sub-carriers, Zero Forcing (ZF) receiver is employed on the received signal in the DCO-GFDM demodulator shown in Fig. 1 as per below expression [7].

$$\hat{\mathbf{d}} = \mathbf{B_{ZF}}\mathbf{y}, \quad (9)$$

where, $\mathbf{B_{ZF}} = (\mathbf{A}^H\mathbf{A})^{-1}\mathbf{A}^H$ is the ZF receiver using the modulation matrix as defined in (5). Alternatively, Minimum Mean Square Error (MMSE) receiver can also be employed for a slightly better response. Eventually, the estimated symbols $\hat{\mathbf{d}}$ are processed further to receive back the transmitted data bits.

III. PERFORMANCE ANALYSIS UNDER CLIPPING NOISE STATISTICS

In this section, we present the analytical expression for BER of DCO-GFDM with the modified electrical SNR under double sided clipping distortion. The inevitable clipping distortion on both sides of the signal due to the non-linear characteristics of the front end device distorts the electrical SNR of the modulated signal. By using (8), the effective electrical SNR per bit (Γ_{eff}) can be written in terms of undistorted electrical SNR per bit $\gamma_{b(elec)} = E_b(ele)/N_0$ as [8],

$$\Gamma_{eff} = \frac{K_f^2}{\xi\left(\frac{R_B\sigma_{clip}^2}{P_{b(elec)}} + \frac{R_B\gamma_{b(elec)}^{-1}}{R_{DC}}\right)}, \quad (10)$$

where, the Noise Enhancement Factor (NEF) ξ on kth sub-carrier is given by,

$$\xi = \sum_{n=0}^{N-1}|[\mathbf{B_{ZF}}]_{k,n}|^2, \quad (11)$$

whose derivation can be found in the Appendix. In addition, $R_B = \frac{M(K-2)}{MK}$ is the bandwidth utilization factor for DCO-GFDM signal, excluding cyclic prefix and cyclic suffix. Similarly, the factor $R_{DC} = \sigma_{x(n)}^2/(\sigma_{x(n)}^2 + P_{bias}^2)$ represents the attenuation of useful electrical power due to the added bias. Further, the analytical expressions for effective attenuation factor K_f and clipping noise power σ_{clip}^2 of DCO-GFDM follows DCO-OFDM and are given as [8],

$$K_f = Q(l_{bottom}) - Q(l_{top}), \quad (12)$$

and,

$$\sigma_{clip}^2 = \sigma_{x(n)}^2(1 - K_f^2) - \triangle\sigma^2, \quad (13)$$

where,

$$\triangle\sigma^2 = \sigma_{x(n)}^2\Big(1 - [Q(l_{bottom}) - Q(l_{top}) + \phi(l_{bottom})l_{bottom}$$
$$- \phi(l_{top})l_{top} + (1 - 2Q(l_{bottom}))l_{bottom}^2 + Q(l_{top})l_{top}^2]$$
$$+ [\phi(l_{bottom}) - \phi(l_{top}) + (1 - Q(l_{bottom}))l_{bottom}$$
$$+ Q(l_{top})l_{top}]^2\Big). \quad (14)$$

Here, $Q(.)$ is complementary cumulative distribution function (CCDF) given by

$$Q(z) = \frac{1}{\sqrt{2\pi}}\int_z^\infty \exp(-\frac{v^2}{2})dv, \quad (15)$$

and $\phi(.)$ is the standard normal distribution. Further, $l_{bottom} = e_{bottom}/\sigma_{x(n)}$ and $l_{top} = e_{top}/\sigma_{x(n)}$ are the normalized bottom and top clipping levels respectively.

Finally, with all the above parameters used for the effective electrical SNR per bit Γ_{eff} in (10), the BER performance of DCO-GFDM for J-QAM under double sided clipping distortion
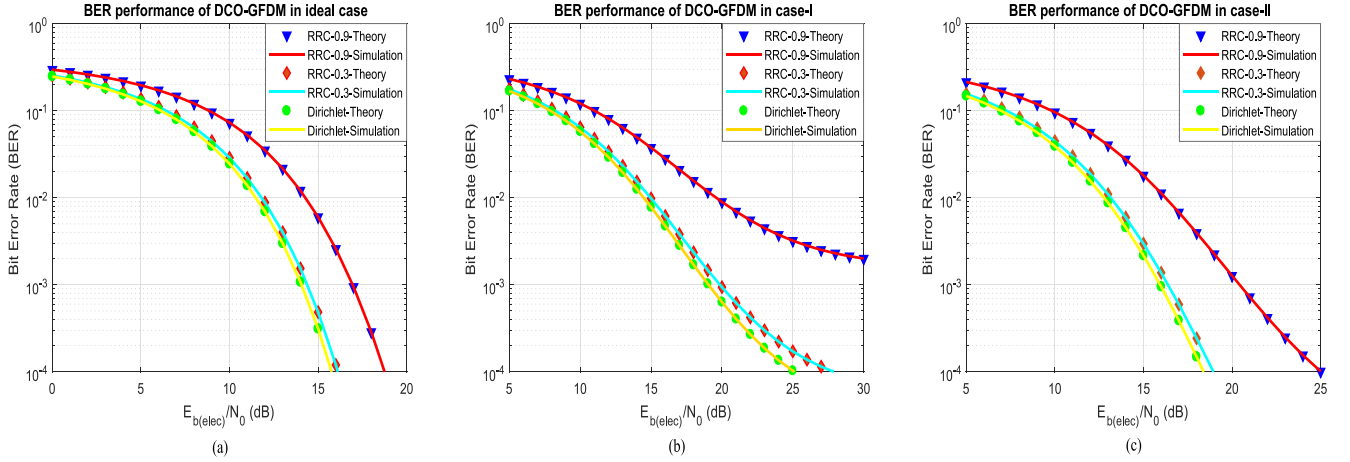
Fig. 4. Comparison of BER performance (simulation vs theory) of DCO-GFDM system under AWGN in different scenarios.

TABLE I
SIMULATION CASES

Parameter	Ideal	Case-I	Case-II
Average optical power (P_{mean}) (mW)	10	10	15
Biasing power (P_{bias}) (mW)	P_{mean}	9.8	14.8
Variance σ_x (mW)	$P_{mean}/2$	4.9	7.4
Lower clipping level (l_{bottom})	-2	-0.98	-1.32
Upper clipping level (l_{top})	∞	8.2	4.76

TABLE II
SIMULATION PARAMETERS

Parameter	Value
Mapping (J)	4-QAM
Number of sub-carriers (K)	256
Number of sub symbols (M)	5
Protype pulse $p(n)$	SRRC with roll-ff (α) Dirichlet,
Monte-Carlo simulations	10,000
LED	VISHAY-TSHG8200
Linear power range (mW)	$P_{min} = 5$ and $P_{max} = 50$

can be given analytically as [8], [11]

$$
BER = 2 \left(\frac{\sqrt{J} - 1}{\sqrt{J} \log_2 J} \right) \text{erfc} \left(\sqrt{\frac{3 \log_2 J}{2(J-1)} . (\Gamma_{eff})} \right)
$$
$$
+ \left(\frac{\sqrt{J} - 1}{\sqrt{J} \log_2 J} \right)^2 \text{erfc}^2 \left(\sqrt{\frac{3 \log_2 J}{2(J-1)} . (\Gamma_{eff})} \right).
\tag{16}
$$

IV. SIMULATION RESULTS

In this section, we present the BER performance investigation of the DCO-GFDM system under the contemplated double sided clipping distortion. The raised clipping noise power due to pre-clipping varies according to normalized top clipping level l_{top} and bottom clipping levels l_{bottom} values which are calculated from the LED front end biasing parameters $\sigma_{x(n)}$ and P_{bias}. Therefore, these clipping levels are set by considering a practical Vishay TSHG8200 LED with a linear range between the power levels $P_{min} = 5$ mW and $P_{max} = 50$ mW, which is done for optical OFDM based systems like in [8], [12]. For the considered LED three different cases are considered for different values of average optical power P_{mean} and biasing power P_{bias}. Accordingly, clipping levels are determined for all the three cases using the procedure as described in Section-II. All the front end biasing parameters for the simulations in different cases with corresponding values for l_{top} and l_{bottom} are presented in Table I which are similar to the cases considered in the BER performance analysis of optical OFDM systems as in [8], [12].

The BER performance of the DCO-GFDM system under the induced clipping distortion is evaluated as a function of altered

effective electrical SNR per bit Γ_{eff} using the undistorted SNR per bit. The robustness of the derived analytical BER expression is verified by using the Monte-Carlo simulations in the MATLAB environment. The BER performance of the DCO-GFDM system is evaluated considering $K = 256$ sub-carriers each transmitting $M = 5$ sub-symbols. The 4-QAM constellation order is taken to study the performance under the three different cases mentioned in Table I. For the circular prototyping pulse $p(n)$ SRRC pulse with roll-off factor α and Dirichlet pulses are examined. The considered system simulation parameters are given in Table II. Soon, the BER performance of the DCO-GFDM system under the ideal case is evaluated with $l_{bottom} = -2$ and $l_{top} = \infty$ and is shown in Fig. 4(a). The simulation results corroborate a close match with theoretical results. Similarly, it can be observed that the BER performance under SRRC degrades with the increase in roll-off factor α. This is imputable to the self interference that takes place among the non-orthogonal sub-carriers. These non-orthogonal sub-carriers increase the NEF (ξ) given in (11) and cause performance degradation. These sub-carriers can be made orthogonal by using Dirichlet pulse which achieves an enhanced performance compared to SRRC pulse and matched to that of DCO-OFDM as in [8], but with more spectral efficiency. This is accomplished because the NEF (ξ) becomes the unity for the Dirichlet pulse.

The BER performance of DCO-GFDM is also evaluated in two more cases with average optical power $P_{mean} = 10$ mW and 15 mW as shown in Fig. 4(b) and (c), respectively. It can be acknowledged that for a specific average optical power within
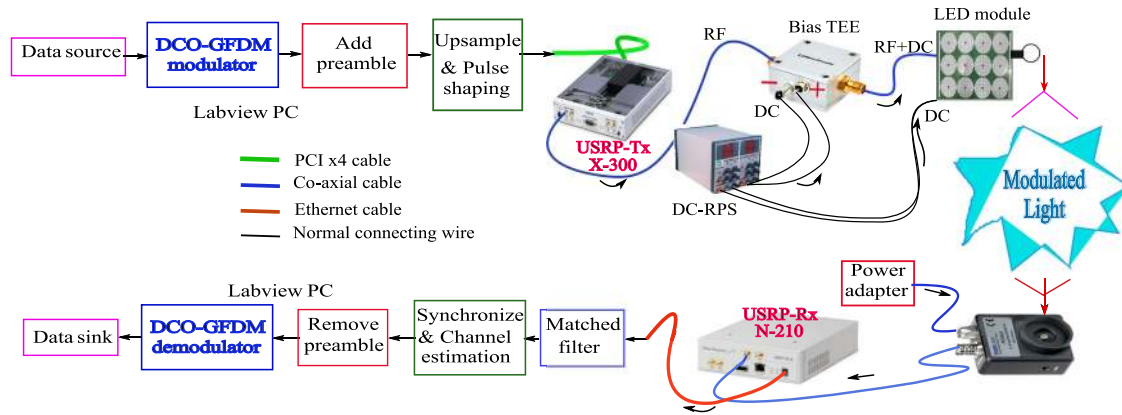
Fig. 5. Deatils of experimental illustration procedure used for DCO-GFDM implementation

TABLE III
EXPERIMENTAL SET-UP PARAMETERS

Name of the parameter	Value	Name of the parameter	Value
Modulation order (J)	4, 16-QAM	Samples in One Frame	6,175
Number of sub carriers (K)	64	USRP IQ sampling rate	4 M
Number of Sub-symbols (M)	5	PD-Thorlabs-PDA8A	(DC-50 MHz), 0.56 A/W @ 820 nm
Number of DCO-GFDM symbols in each packet	4	LED	3 W
Null carriers	25 % of K	Link distance	0.5 m
Preamble and zero pad length	256	Average electrical transmitted power (mW)	4
Pulse shaping (RRC) length	8	USRP with LFTx and LFRx daughter boards	Ettus X300, N210
Oversampling factor (L)	4	Bias Tee	ZFBT-6GW-FT+

the given dynamic range of LED, a lower bias value results in more clipping and gives a poorer performance as in the Case-I showed in Fig. 4(b). Further, we can observe that by shifting the bias P_{bias} towards the center of the dynamic range as in case-II, the amount of clipping noise decreases, thereby improving the performance compared to case-I as depicted in Fig. 4(c). Moreover, the relative performance between SRRC pulse and Dirichlet is similar to that of the ideal case. Importantly, in these cases also, simulation and theoretical results confirm a close match. In conclusion, it can be inferred that for DCO-GFDM also a front end device with more average optical power in the given dynamic range is preferred which is alike DCO-OFDM as stated in [8]. In the following part, we manifest the experimental proof of the DCO-GFDM system using the USRP based test bed.

V. EXPERIMENTAL RESULTS

The details of various processing steps involved in the experimental validation of DCO-GFDM system with the corresponding hardware is illustrated in Fig. 5. The baseband modulation and other processing steps required to overcome channel anomalies are performed by using Lab-view software. The Ettus USRP x300 is used as a transmitter board and N210 is made as a receiver USRP with LFTx and LFRx daughter boards, respectively. The details of various parameters exerted in the experimentation are listed in Table III. The DCO-GFDM system is considered to have $K = 64$ sub-carriers and $M = 5$ sub-symbols on each sub-carrier. In each data packet, 4 DCO-GFDM symbols are transmitted along with a pre-amble and double sided zero-padding constituting together 256 samples. This total frame is
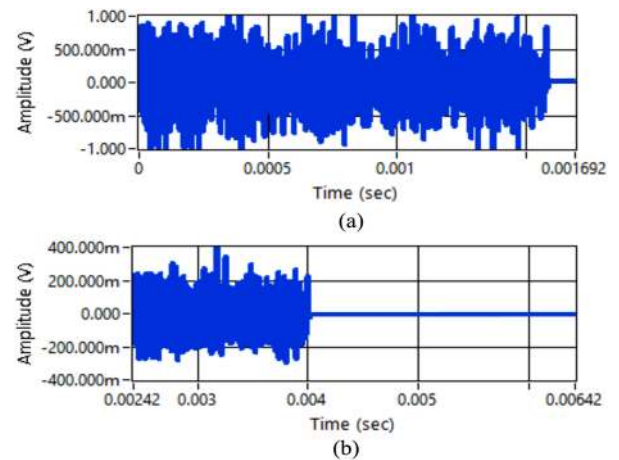

Fig. 6. An illustration of time domain signals. (a) Transmitted data packet. (b) Received data packet

pulse shaped with a filter of length 8 samples and oversampled by a factor equal to 4. The baseband discrete signal, thus generated is given to transmitter USRP which reconverts the signal into In-phase (I)/ Quad-phase (Q) form according to the specified IQ sampling rate of 4 M samples per second. It should be noted that the Q-component is zero as we give a pure real signal to USRP. This IQ signal's I component of the transmitted data packet is shown in Fig. 6(a). The duration of the packet is 1.543 ms determined by dividing the frame length with IQ rate. Thereafter, the USRP up-converts the signal to the desired RF frequency at 20 MHz and then transmits it to the bias tee where a DC bias
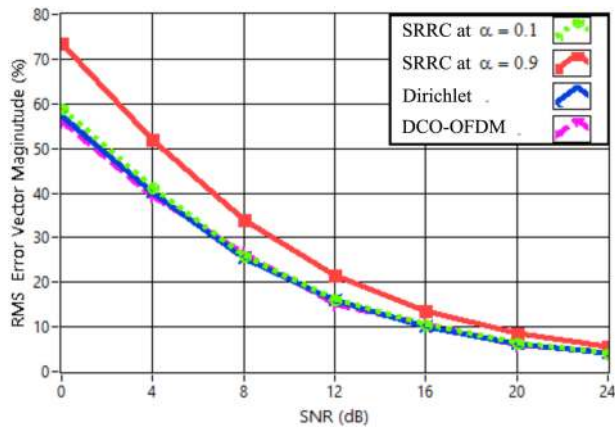
Fig. 7. EVM performance comparison for 4-QAM of DCO-GFDM in different cases
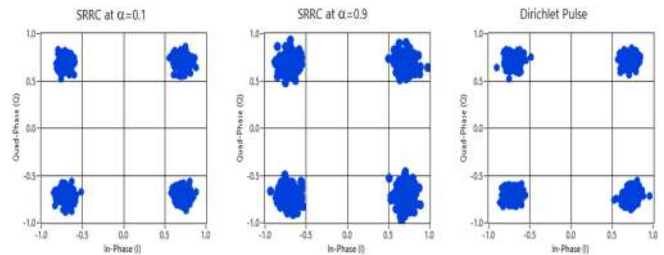

Fig. 8. Received constellations for 4-QAM in different cases of DCO-GFDM at an SNR = 18 dB

Fig. 9. Received constellations for 16-QAM in different cases of DCO-GFDM at an SNR = 18 dB

is added to make it to unipolar signal. This unipolar signal is then utilized to drive the LEDs in the limited linear portion of its characteristics and modulate the light intensity. Subsequently, on the receiver side, the intensity modulated light is collected by using a Thorlabs Photodiode PDA8A and an electrical signal is generated which is amplified by an inbuilt trans-impedance amplifier. After being amplified, the signal is received by receive USRP which down converts the signal and generates data packet as shown in Fig. 6(b) according receiver IQ rate. It can be immediately noticed that there is a delay and attenuation in the signal due to propagation, but no change in the duration. However, to retrieve the packet the capture time must be at least 10 times longer enough than its duration. The detected packet is then processed by the LabView PC where the packet is undergone matched filtering, synchronization, and channel estimation as shown in Fig. 5. In the present work, traditional synchronization like Schmidl and Cox algorithm, and Minimum Mean Square Error (MMSE) estimation for the channel are applied [9]. Soon after the DCO-GFDM demodulator demodulates the packet and retrieves estimated QAM symbols. Eventually, the data bits are recovered from the estimated QAM symbols by the de-mapper.

Predominantly, the validation of the proposed real time DCO-GFDM system in the work is accomplished by Root Mean Square (RMS) Error Vector Magnitude (EVM), received constellations and received magnitude spectrums in comparison to DCO-OFDM system. We investigate the comparative performance with SRRC pulse and Dirichlet pulses for 4-QAM and 16-QAM. The RMS-EVM used in the comparative analysis is computed by,

$$EVM(\%) = \sqrt{\frac{\frac{1}{N}\sum_{n=0}^{N-1}[(I_n - \hat{I}_n)^2 + (Q_n - \hat{Q}_n)^2]}{\frac{1}{N}\sum_{n=0}^{N-1}[I_n^2 + Q_n^2]}} \times 100. \tag{17}$$

In (17), I_n and Q_n are the in-phase and quadrature phase values of ideal symbols, whereas $\hat{I}_n$ and $\hat{Q}_n$ are the in-phase and quadrature phase values of receiving symbols. The comparison of RMS-EVM (%) variation with respect to SNR (dB) between DCO-GFDM and DCO-OFDM is depicted in Fig. 7 for 4-QAM constellation. The DCO-OFDM system under consideration is
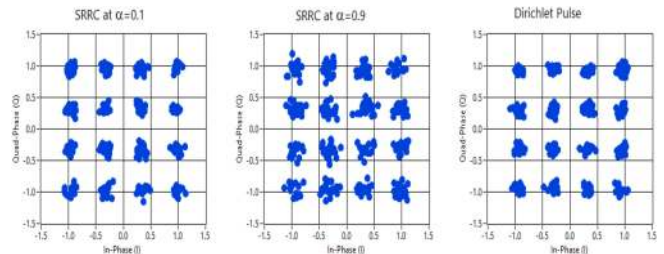
implemented with the same number of sub-carriers $K = 64$ as that of DCO-GFDM but with $M = 1$ which means at lower spectral efficiency. From Fig. 7, we can observe the variation of EVM for the two candidate pulses SRRC and Dirichlet in the DCO-GFDM system. It can be immediately noticed that lower values of EVM are obtained at low SNR values in DCO-GFDM using SRRC at a low value of $\alpha = 0.1$ compared to $\alpha = 0.9$. However, the use of SRRC pulse destroys the orthogonality among the sub-carriers, which will increase self-interference among them. Therefore, Dirichlet pulse is applied to improve orthogonality among sub-carriers in DCO-GFDM and lower values of EVM are achieved similar to DCO-OFDM, but at more spectral efficiency. In particular, the measured EVM of DCO-GFDM at an SNR of 12 dB using SRRC with $\alpha = 0.9$ is nearly 22% and is reduced to around 15% by using SRRC with $\alpha = 0.1$ and Dirichlet pulse. This is similar to the performance of DCO-OFDM but at more spectral efficiency, which is attained due to the transmission of multiple symbols on each sub-carrier in the DCO-GFDM system. The deviation in the EVM performance can be noticed in the received constellations shown in Fig. 8 and Fig. 9 for 4-QAM and 16-QAM for DCO-GFDM under different cases. Similar trends for the EVM are noticed for 16-QAM for all the cases under consideration in all the systems, but at slightly increased levels around $2-3\%$ due to a higher order constellation. However, these EVM results are not shown to limit the paper size.

Further, the comparison between the magnitude spectrums of DCO-GFDM and DCO-OFDM is evaluated and depicted in Fig. 10. The number of sub-carriers and the null carriers are taken as per the values mentioned in the Table III. To make a fair comparison, the number of samples per frame in both systems is made equal. In each subplot of Fig. 10, the transmitted and received spectrum of the corresponding modulation is depicted.
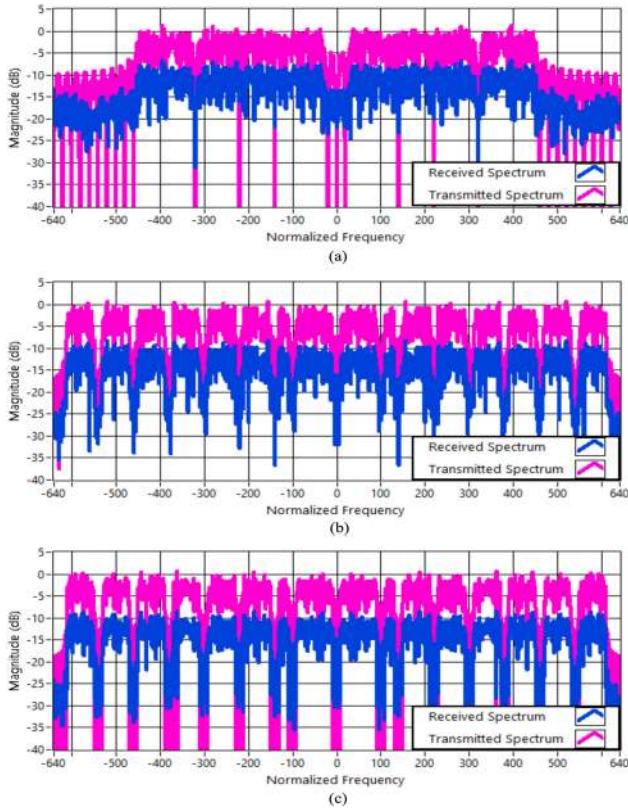
Fig. 10. Comparison between transmitted and received spectrums of (a) DCO-OFDM, (b) DCO-GFDM with Dirichlet pulse, and (c) DCO-GFDM with SRRC at $\alpha = 0.1$

TABLE IV
EXPERIMENTALLY ACHIEVED RESULTS IN DIFFERENT CASES

System type	BER		Estimated SNR	OOB
	SNR=5dB	SNR=20dB		[dB]
DCO-GFDM with SRRC at $\alpha = 0.9$	0.3578	1.129×10^{-3}	21.18	-14.8
DCO-GFDM with SRRC at $\alpha = 0.1$	0.2443	3.223×10^{-4}	23.42	-19.2
DCO-GFDM with Dirichlet	0.2325	2.186×10^{-4}	24.26	-16.2
DCO-OFDM	0.2428	2.926×10^{-4}	24.82	-10

We can notice that the amplitude of the received spectrum in all the subplots is distorted which is due to channel anomalies. More importantly, we note that the Out Of Band (OOB) emission in DCO-OFDM is -10 dB whereas in DCO-GFDM it is reduced to a minimum of -16.2 dB which explicitly shows the power efficiency of DCO-GFDM system. To be specific, in DCO-GFDM using SRRC with $\alpha = 0.1$ gives -19.2 dB OOB which is 3 dB less to that of using Dirichlet pulse. This is due to the deeper side lobes that occur in the SRRC for lower values of α. For an easy interpretation, the experimentally achieved results in different cases are listed in Table IV which gives BER, estimated SNR at receiver along with OOB. The estimated SNR at the receiver is an important parameter computed by using mean square error in channel estimation and it reflects the detection

accuracy. The Table IV shows good estimated SNR values which corroborate the better detection capability of the implemented real time system.

VI. CONCLUSION

In this paper, the performance analysis of a recently explored VLC multi-carrier waveform named DCO-GFDM is studied under the double sided induced clipping distortion and demonstrated the real time implementation of the corresponding waveform in VLC systems for the first time using two different prototype pulses. The simulation results for BER confirms a close match to that of theoretical results. Further, the experimentally achieved results for RMS-EVM and BER for DCO-GFDM with SRRC at lower roll-off and Dirichlet pulse manifest the same performance to that of DCO-OFDM, but at more power efficiency and spectral efficiency along with the extra flexibility in the waveform generation. Besides, the better estimated SNR at the receiver shows good detection accuracy. In summary, DCO-GFDM is an appropriate successor for DCO-OFDM and can rise as a desirable waveform for the growing 5 G based VLC technology.

APPENDIX

This appendix presents the derivation of NEF (ξ) which can be obtained from (8) and (9). The estimated data symbols after substituting (8) in (9) can be written as,

$$\hat{\mathbf{d}} = \mathbf{B}_{\mathbf{ZF}}[g_{opt}K\mathbf{x} + g_{opt}\mathbf{w}_{\mathbf{clip}} + \mathbf{w}], \qquad (18)$$

To obtain NEF, we need to calculate the variance of estimated symbols as,

$$\mathbb{E}\{\hat{\mathbf{d}}\hat{\mathbf{d}}^H\} = \mathbb{E}\left[(\mathbf{B}_{\mathbf{ZF}}\mathbf{x} + \mathbf{B}_{\mathbf{ZF}}\mathbf{w}_{\mathbf{clip}} + \mathbf{B}_{\mathbf{ZF}}\mathbf{w}) \right.$$
$$\left. (\mathbf{B}_{\mathbf{ZF}}\mathbf{x} + \mathbf{B}_{\mathbf{ZF}}\mathbf{w}_{\mathbf{clip}} + \mathbf{B}_{\mathbf{ZF}}\mathbf{w})^H\right],$$

in which $\mathbb{E}$ denotes the expectation operator the constants are omitted for the sake of simplicity which does not affect the analytical part. Since the noise components $\mathbf{w}_{\mathbf{clip}}$ and $\mathbf{w}$ are independent as stated in the Section-II, (18) is simplified to,

$$\mathbb{E}\{\hat{\mathbf{d}}\hat{\mathbf{d}}^H\} = \underbrace{\mathbb{E}(\mathbf{B}_{\mathbf{ZF}}\mathbf{x}\mathbf{x}^H\mathbf{B}_{\mathbf{ZF}}^H)}_{1} + \underbrace{\mathbb{E}(\mathbf{B}_{\mathbf{ZF}}\mathbf{w}_{\mathbf{clip}}\mathbf{w}_{\mathbf{clip}}^H\mathbf{B}_{\mathbf{ZF}}^H)}_{2}$$
$$+ \underbrace{\mathbb{E}(\mathbf{B}_{\mathbf{ZF}}\mathbf{w}\mathbf{w}^H\mathbf{B}_{\mathbf{ZF}}^H)}_{3}, \qquad (19)$$

in which the remaining terms are vanished due to uncorrelated nature. In (19), first term constitutes signal power, whereas second and third terms constitute noise power. So considering only the noise part leads to,

$$\mathbb{E}(\mathbf{B}_{\mathbf{ZF}}\mathbf{w}_{\mathbf{clip}}\mathbf{w}_{\mathbf{clip}}^H\mathbf{B}_{\mathbf{ZF}}^H) + \mathbb{E}(\mathbf{B}_{\mathbf{ZF}}\mathbf{w}\mathbf{w}^H\mathbf{B}_{\mathbf{ZF}}^H)$$
$$= \mathbf{B}_{\mathbf{ZF}}\mathbf{B}_{\mathbf{ZF}}^H\sigma_{clip}^2 + \mathbf{B}_{\mathbf{ZF}}\mathbf{B}_{\mathbf{ZF}}^H\sigma_w^2$$
$$= \mathbf{B}_{\mathbf{ZF}}\mathbf{B}_{\mathbf{ZF}}^H\underbrace{(\sigma_{clip}^2 + \sigma_w^2)}_{Noise\,power}$$
$$= \xi \times \text{noise power},$$

which means that the noise power is increased by factor ξ, which is termed as Noise Enhancement Factor (NEF). This NEF considering the kth sub-carrier is given by (11) as,

$$\xi = \sum_{n=0}^{N-1} |[\mathbf{B_{ZF}}]_{k,n}|^2.$$

REFERENCES

[1] M. Ayyash *et al.*, "Coexistence of WiFi and LiFi toward 5G: Concepts, opportunities, and challenges," *IEEE Commun. Mag.*, vol. 54, no. 2, pp. 64–71, Feb. 2016.

[2] H. Haas, L. Yin, Y. Wang, and C. Chen, "What is LiFi?," *J. Lightw. Technol.*, vol. 34, no. 6, pp. 1533–1544, Mar. 2016.

[3] H. Haas and T. Cogalan, "LiFi opportunities and challenges," in *Proc. 16th Int. Symp. Wireless Commun. Syst.*, 2019, pp. 361–366.

[4] A. Cailean and M. Dimian, "Current challenges for visible light communications usage in vehicle applications: A survey," *IEEE Commun. Surveys Tuts.*, vol. 19, no. 4, pp. 2681–2703, Oct.–Dec. 2017.

[5] H. Elgala, R. Mesleh, H. Haas, and B. Pricope, "OFDM visible light wireless communication based on white leds," in *Proc. IEEE 65th Veh. Technol. Conf.*, 2007, pp. 2185–2189.

[6] V. Kishore and V. Mani, "A DC biased optical generalised frequency division multiplexing for IM/DD systems," *Phys. Commun.*, vol. 33, pp. 115–122, 2019.

[7] V. Kishore and V. Mani, "An LED modelled GFDM for optical wireless communications," *AEU - Int. J. Electron. Commun.*, vol. 101, pp. 54–61, 2019.

[8] S. Dimitrov, S. Sinanovic, and H. Haas, "Clipping noise in OFDM-based optical wireless communication systems," *IEEE Trans. Commun.*, vol. 60, no. 4, pp. 1072–1081, Apr. 2012.

[9] S. P. Valluri, "Investigation of blind CFO estimation for GFDM system using universal software radio peripheral: Theory, simulations and experiments," *IET Commun.*, vol. 13, no. 13, pp. 1936–1944, Aug. 2019.

[10] K. Vejandla, S. Valluri, V. M. Vakamulla, and A. Kumar, "A tunable energy signal for intensity modulation and direct detection systems: Theory, simulations, and experiments," *IEEE Photon. J.*, vol. 12, no. 1, pp. 1–12, Feb. 2020.

[11] N. Michailow *et al.*, "Generalized frequency division multiplexing for 5th generation cellular networks," *IEEE Trans. Commun.*, vol. 62, no. 9, pp. 3045–3061, Sep. 2014.

[12] K. Vejandla, S. Kollikonda, and V. M. Vakamulla, "Performance analysis of PAM-DMT under double sided signal clipping in IM/DD based systems," in *Proc. Nat. Conf. Commun. (NCC)*, 2020, pp. 1–6.

[13] J. A. Rice, *Mathematical Statistics and Data Analysis*, 2nd ed. Pacific Grove, CA, USA: Duxbury Press, 1995.

[14] J. J. Bussgang, "Crosscorrelation functions of amplitude-distorted Gaussian signals," Research Laboratory of Electronics, Massachusetts Institute of Technology, Cambridge, MA, USA, Tech. Rep. 216, Mar. 1952.

Vejandla Kishore (Student Member, IEEE) received the B.Tech. degree in electronics and communication engineering from Jawaharlal Nehru Technological University-Hyderabad, Hyderabad, India and the M.Tech. degree in digital systems and signal processing from the Gandhi Institute of Technology and Management, Visakhapatnam, India, in 2008 and 2013, respectively. He is currently working toward the Ph.D. degree with the National Institute of Technology, Warangal, Fathimanagar, India. His research interests include signal processing for optical wireless communications, communications with major emphasis on modulation and broadband optical wireless communications, and designing real-time test bed design for visible light communication.

Siva Prasad Valluri (Student Member, IEEE) received the B.Tech. and M.Tech. degrees in 2011 and 2016, respectively, and the Ph.D. degree in wireless communications from the National Institute of Technology Warangal, Fathimanagar, India, in 2020. He is currently working as an Assistant Professor with SRKR Engineering College, Bhimavaram, India. His research interests include signal processing for communications, communications with major emphasis on modulation and broadband wireless communications, and designing real-time test bed.

Venkata Mani Vakamulla (Senior Member, IEEE) received the B.Eng. and M.Eng. degrees in electronics and communication engineering from Andhra University, Visakhapatnam, India, in 1992 and 2003, respectively, and the Ph.D. degree from the Indian Institute of Technology (IIT) Delhi, Delhi, India, in 2009. She is currently an Associate Professor with the Department of Electronics and Communication Engineering, National Institute of Technology Warangal, Fathimanagar, India. Her areas of interest include wireless communication, signal processing for communications, software defined radio, networking, Localization and positioning, and visible light communication.

Mathini Sellathurai (Senior Member, IEEE) is a Full Professor in signal processing and intelligent systems with Heriot-Watt University, Edinburgh, U.K. In her 15-year research on Signal Processing for Communications, she has made seminal contributions to MIMO wireless systems. She has authored 200 IEEE entries, given invited talks, and has written a book and several book chapters in topics related to this project. She was the recipient of the IEEE Communication Society Fred W. Ellersick Best Paper Award in 2005, Industry Canada Public Service Award for contributions to science and technology in 2005, and the Best Ph.D. thesis medal from NSERC Canada in 2002. She is also a member for IEEE SPCOM Technical Strategy Committee (2014–2018), Editor for the IEEE TRANSACTIONS ON SIGNAL PROCESSING (2009–2014, 2015–2018). She was also the General Co-Chair of IEEE International Workshop on Signal Processing Advances in Wireless Communications, 2016, Edinburgh.

Abhinav Kumar (Senior Member, IEEE) received the B.Tech., M.Tech., and Ph.D. degrees in electrical engineering from the Indian Institute of Technology Delhi, Delhi, India, in 2009 and 2013, respectively. In 2013, he was a Research Associate with the Indian Institute of Technology Delhi. From 2013 to 2014, he was a Postdoctoral Fellow with the University of Waterloo, Canada. Since November 2014, he has been with the Indian Institute of Technology, Hyderabad, India, where he is currently an Associate Professor. His research interests are in the different aspects of wireless communications and networking.

Tharmalingam Ratnarajah (Senior Member, IEEE) is currently with the Institute for Digital Communications, The University of Edinburgh, Edinburgh, U.K., as a Professor in digital communications and signal processing. He has supervised 15 Ph.D. students and 21 Postdoctoral Research Fellows, and raised more than 11 million USD of research funding. He was the Coordinator of the EU projects ADEL (3.7M) in the area of licensed shared access for 5G wireless networks, HARP (4.6M) in the area of highly distributed MIMO, the EU Future and Emerging Technologies projects HIATUS (3.6M) in the area of interference alignment, and CROWN (3.4M) in the area of cognitive radio networks. He has authored more than 400 articles in these areas and holds four U.S. patents. His research interests include signal processing and information theoretic aspects of 5G and beyond wireless networks, full-duplex radio, mmWave communications, random matrix theory, statistical and array signal processing, and quantum information theory. He was an Associate Editor for the IEEE TRANSACTIONS ON SIGNAL PROCESSING, from 2015 to 2017, and the Technical Co-Chair in the 17th IEEE International Workshop on Signal Processing Advances in Wireless Communications, Edinburgh, in 2016. He is a Fellow of the Higher Education Academy.